Interaction of CO with PdAu(111) and PdAu(100) Bimetallic Surfaces: A Theoretical Cluster Model Study

ARTICLE *in* THE JOURNAL OF PHYSICAL CHEMISTRY C · APRIL 2008

Impact Factor: 4.77 · DOI: 10.1021/jp710915g

4 AUTHORS:

Gloria Mazzone
Università della Calabria
24 PUBLICATIONS **163** CITATIONS
SEE PROFILE

Ivan Rivalta
Yale University
57 PUBLICATIONS **595** CITATIONS
SEE PROFILE

Nino Russo
Università della Calabria
511 PUBLICATIONS **7,939** CITATIONS
SEE PROFILE

Emilia Sicilia
Università della Calabria
151 PUBLICATIONS **1,942** CITATIONS
SEE PROFILE

Interaction of CO with PdAu(111) and PdAu(100) Bimetallic Surfaces: A Theoretical Cluster Model Study

Gloria Mazzone, Ivan Rivalta, Nino Russo, and Emilia Sicilia*

Dipartimento di Chimica and Centro di Calcolo ad Alte Prestazioni per Elaborazioni Parallele e Distribuite−Centro d'Eccellenza MURST, Università della Calabria, I-87030 Arcavacata di Rende, Italy

Received: November 15, 2007; In Final Form: January 10, 2008

Structural parameters, binding energies, and bonding mechanism of CO molecules on PdAu(111) and PdAu(100) surface alloys have been investigated at the density functional level by employing a cluster model approach. Cluster models have been constructed to represent second-neighbor Pd pairs on both the exposed gold surfaces, given that special ensembles are able to confine reactants in a small region of bimetallic catalysts. Analysis of the cluster size dependence of the chemisorption properties has been carried out together with the study of the influence of exchange correlation functional and basis set quality. An accurate description of the bonding mechanism of CO on top of Pd monomers surrounded by gold atoms has been achieved by an atom-projected description of the surface bond. The remarkable agreement of computed results with available experimental information and previous periodic supercell calculations clearly indicates that the adopted cluster models are suitable for chemisorption studies on PdAu surface alloys.

1. Introduction

The selectivity and efficiency of catalytic processes can be largely enhanced by use of bimetallic instead of monometallic catalysts.[1−4] The concepts of "ensemble" (or geometric)[5,6] and "ligand" (or electronic)[7] effects are commonly used to rationalize this superior activity of bimetallic systems in electrochemistry and heterogeneous catalysis. The former concept refers to the fact that the addition of a second metal may block certain sites, reducing or eliminating the formation of an inhibiting species or an important intermediate. Thus, specific groupings of surface atoms are required to serve as active sites.[1,5,6] The latter effect refers to the formation of heteronuclear metal−metal bonds in binary alloys that involves a modification of the electronic structure, leading to a different (and, it is hoped, better) overall catalytic activity with respect to that of either of the constituent metals. Orbital rehybridization of one or both of the metals and/or charge transfer between the metals can substantially modify the catalytic performance by means of ligand effect.[1,7]

Among bimetallic systems, Pd−Au has received particular attention due to its use in a number of catalytic reactions (e.g., CO oxidation, cyclotrimerization of acetylene, synthesis of vinyl acetate monomer, selective oxidation of alcohols to aldehydes)[8−11] and applications (e.g., hydrogen fuel cells and pollution control systems).[12−13] A deeper understanding of the underlying physical reasons that determine the catalytic performance of Pd−Au alloys can thus be very beneficial for rational improvement of these catalysts.

The utility of single-crystal studies for understanding the role played by ensemble and ligand effects in bimetallic catalysts has been demonstrated[14] because they are simple enough for a systematic study of the relationship between the microscopic structure of the catalyst and its activity. At the same time, a broad variety of possible compositions and structures of increasing complexity can be examined. Therefore, well-defined bimetallic Pd−Au surfaces have been the subject of several investigations.[15−19]

Goodman and co-workers,[5] in their investigations of the promotional role of gold in a palladium−gold alloy catalyst used for the acetoxylation of ethylene to yield vinyl acetate (VA), have invoked ensemble effects to explain the significant enhancement of the VA formation rate. The ligand and eventually strain effects have been considered minimal and a pair of noncontiguous Pd monomer sites has been supposed to be the critical ensemble for the VA formation as inferred from the difference in the VA formation rates on Pd/Au(100) and Pd/Au(111) surfaces.

Surface composition is, therefore, the key to understanding the catalytic properties of bimetallic surface alloys, especially for the catalytic systems for which the efficiency and selectivity are dominated by the ensemble effect. In fact, the surface segregation in Pd−noble metal alloys is well-known by both experimental evidence for Pd−Cu,[21] Pd−Ag,[22] and Pd−Au[23,24] and theoretical periodic calculations.[25] Since the morphology of Pd−Au strongly depends on the experimental preparation in terms of deposition technique and annealing history, several Pd−Au surface compositions have been reported so far.[5,6,9,26−28]

The use of the in situ STM technique developed by Behm and co-workers[6] has allowed the determination of critical ensembles for adsorption of small molecules. Application of this technique has shown that the critical ensemble for CO adsorption on PdAu(111) surface-alloy electrodes is a Pd monomer.

The adsorption of small molecules, such as CO, is commonly used to obtain information concerning the properties of single-metal and alloy surfaces, including composition and electronic structure, by both experimental and theoretical studies.

The contribution given by first-principles calculations to better microscopic understanding of the catalytic activity of bimetallic systems has been recently reviewed by Gross,[29] showing how theoretical calculations can supply additional information for the rational design of robust bimetallic catalysts.[30−32]

* Corresponding author: e-mail siciliae@unical.it.

10.1021/jp710915g CCC: $40.75
Published on Web 03/20/2008

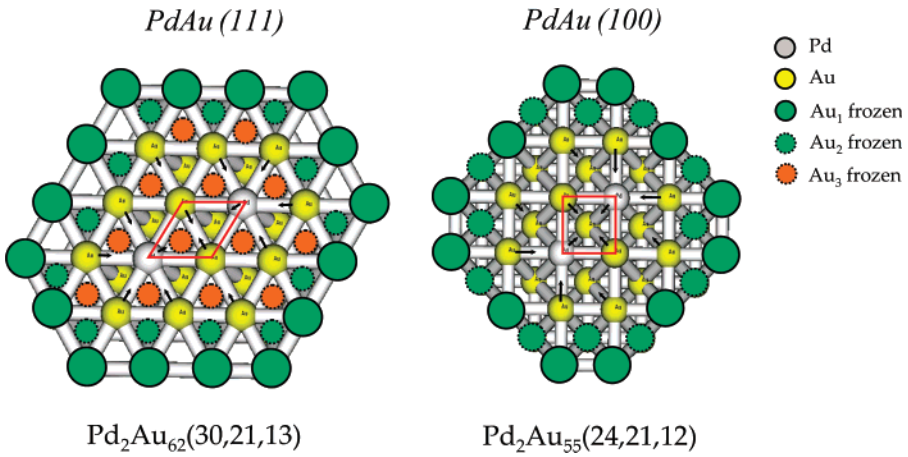

Figure 1. Schematic representation of Pd_2Au_n clusters used in this work to model the second-neighbor Pd pair ensemble on PdAu(100) and PdAu(111) surface alloys. From the top view, the positions of the frozen Au_3 atoms are not directly visible in the fcc(100) surface cluster model due to its ABAB packing, but they correspond to the unfrozen atoms in the first layer. Changes in the atomic positions due to the local relaxation are indicated by arrows. Unit cells of the Au(100) and Au(111) pure surfaces are depicted in red.

In the framework of density functional (DF) calculations, the periodic supercell approach using plane-waves has already been applied to PdAu surface alloys for the study of the surface segregation phenomenon and of the atomic configuration of Pd atoms in PdAu(111) bimetallic surfaces.[25,33] On the other hand, the cluster model approach has provided information about several catalytic systems[34] and has proved to be a useful tool for surface science studies. For the study of chemisorption properties of CO on low-index surfaces, cluster model calculations can be compared with periodic calculations[35] and can be used to focus on the chemical bonding between the surface atoms and the adsorbed molecule.[36,37] Nevertheless, few examples of the application of the cluster model approach in bimetallic systems can be found in literature, such as for PtRe,[38] PdCu,[39,40] and PdSn, RhSn, and RhZn[41] catalysts.

A DF cluster model approach has been applied here to the study of the adsorption properties of CO on the PdAu(111) and PdAu(100) surface alloys. In particular, cluster models have been built up to represent the ensemble with a second-neighbor Pd pair on both the exposed gold surfaces, given that ensembles with second-neighbor Pd appear to be seldom separated from isolated monomers.[42]

The calculated energetic, electronic, and vibrational properties will be compared with the recent periodic calculations for PdAu(111)[33] and with the available experimental data.

2. Methodology and Computational Details

In the cluster approach the adsorption site is modeled by a finite number of metal atoms whose arrangement is chosen to properly reproduce those contributions to the adsorbate−substrate interaction that are due to local changes in the substrate electronic structure. Thus, it is reasonable to expect that cluster models are able to capture the essential features of the chemisorption bond and to predict local properties such as adsorption geometries and vibrational frequencies for very low coverages.

In order to model the second-neighbor Pd pair ensemble on PdAu(100) and PdAu(111) surfaces, we have built up the clusters starting with a group of two noncontiguous Pd atoms and two Au atoms bonded to both of them. Then, the first neighbors of those four atoms have been added both in the first and in the second layer. In this way, the active sites are represented by Pd_2Au_{19} and Pd_2Au_{20} cluster models, denoted as Pd_2Au_{19}(12,9) and Pd_2Au_{20}(14,8) to indicate the number of atoms in each cluster layer for Au(100) and Au(111) surfaces, respectively.

Initially, the atomic positions have been assigned as in bulk gold, with the experimental lattice parameter of 4.08 Å, yielding an Au−Au (initially equal to Pd−Au) distance of 2.885 Å.

With these models a good description of the coordination of the two noncontiguous Pd monomers involved in the chemisorption sites for both low-index gold surfaces is obtained.

In order to study the influence of the cluster size on the geometry and energetics of adsorbed CO, we have used the strategies that will be illustrated below.

First, the size of the Pd_2Au_{19}(12,9) model has been increased by adding a third layer in such a way to obtain for the PdAu(100) surface the Pd_2Au_{23}(12,9,4) cluster, including in the third layer four gold atoms that lie in the positions corresponding to those of the four central atoms in the first layer, because of the ABAB packing of the fcc(100) surface. For the less open fcc(111) gold surface with ABCABC packing, eight atoms have been added in the third layer to the Pd_2Au_{20}(14,8) model in correspondence to the atomic positions defining the fcc-hollow adsorption sites, giving rise to the larger Pd_2Au_{28}(14,8,8) cluster.

Starting from these three-layer models, two more extended clusters have been constructed by completing the set of the first neighbor atoms for all the peripheral atoms of the first and the second layer. The resulting Pd_2Au_{55}(24,21,12) and Pd_2Au_{62}(30,21,13) large models for the Pd/Au(100) and the Pd/Au(111) systems, respectively, would prevent any indirect insaturation effect for the two noncontiguous Pd and the two Au atoms of the active sites. Moreover, these large models have been used to take into account local relaxation effects due to the substitution of two noncontiguous surface gold atoms with two Pd monomers. The positions of the atoms defining the Pd_2Au_{19}(12,9) and Pd_2Au_{20}(14,8) models have been fully optimized; in fact, within the Pd_2Au_{55}(24,21,12) and Pd_2Au_{62}(30,21,13) clusters the positions of the remaining atoms are frozen (Figure 1). Finally, the Pd_2Au_{19}(12,9), Pd_2Au_{23}(12,9,4) and the Pd_2Au_{20}(14,8), Pd_2Au_{28}(14,8,8) models have been pulled out from the corresponding partially optimized Pd_2Au_{55} and Pd_2Au_{62} clusters.

In summary, the relaxed Pd_2Au_{19}, Pd_2Au_{23}, and Pd_2Au_{55} models for the Pd/Au(100) surface and Pd_2Au_{20}, Pd_2Au_{28}, and Pd_2Au_{62} models for the Pd/Au(111) surface have been employed to study the chemisorption properties of CO.

In order to explore the variation of the electronic structure of gold surfaces due to the substitution of two noncontiguous gold atoms by two Pd monomers on Au(111) and Au(100) clean surfaces, six Au_{n+2} cluster models corresponding to the Pd_2Au_n models described above have been used. As for the bimetallic clusters, the largest Au_{n+2} cluster models have been locally relaxed, starting from the bulk gold atomic positions, and then the smaller Au_{n+2} models have been pulled out from them.

The calculations have been performed with the Turbomole package (version 5.8)[43] at the DF level, by use of the BP86 functional[44,45] within the resolution of the identity approximation for computing the electronic Coulomb interaction (RI-J). This approach expands the molecular electron density in a set of atom-centered auxiliary functions, improving the computational efficiency of large-scale calculations.[46,47]

The Stuttgart effective core potential[48] have been used to model the scalar relativistic effects, replacing the 28 and 60 core electrons of palladium and gold atoms, respectively. The valence electrons, 18 for Pd and 19 for Au, have been explicitly considered in the standard Turbomole SVP basis set.[49] For CO, the all-electron SVP basis set of Ahlrichs and co-workers,[49] featuring a split valence basis set with polarization functions, has been employed. The standard Turbomole SVP auxiliary basis set has been used for all the atoms.[47]

No symmetry constraints have been imposed for the relaxation of the positions of C and O atoms in the adsorption study of one and two CO molecules on the Pd_2Au_n cluster models.

For selected CO/Pd_2Au_{19}(12,9) and CO/Pd_2Au_{28}(14,8,8) cluster models, the influence of the exchange−correlation (xc) functional and basis set effect on vibrational frequencies, geometries, and binding energies of the adsorbate have also been investigated. Becke's three-parameter hybrid functional[50] combined with the Lee, Yang, and Parr (LYP)[51] correlation functional, the standard Turbomole TZVP basis set,[52] and the corresponding auxiliary basis set[47] for C and O atoms have been employed for this purpose. From now on, for the sake of clarity, the four levels of theory used in this work will be indicated as BP86/SVP and BP86/TZVP for the pure (i.e., nonhybrid) xc functional and B3LYP/SVP and B3LYP/TZVP for the hybrid B3LYP functional.

It should be emphasized that the Pd_2Au_{19}(12,9) and Pd_2Au_{28}(14,8,8) cluster models used to calculate the chemisorption properties of CO at the B3LYP level have been obtained by partially optimizing the larger Pd_2Au_{55} and Pd_2Au_{62} models at the same level of theory, following the same strategy described above.

All the C−O stretching frequencies reported in this work have been corrected by use of scaling factors, calculated with respect to the C−O vibrational frequency for the isolated CO molecule in the gas phase obtained at the corresponding level of theory. Scaling factors applied to the C−O frequencies in the chemisorbed systems are 1.0084 (BP86/SVP), 1.0197 (BP86/TZVP), 0.9679 (B3LYP/SVP), and 0.9792 (B3LYP/TZVP).

The total energies calculated after geometry optimizations have been corrected for basis-set superposition error (BSSE) by use of Boys−Bernardi counterpoise calculations[53] for all adsorbate/cluster models. This correction is 3.3 kcal/mol per bond for all the cluster models if the SVP basis set is used, whereas is only 1.0 kcal/mol when the triple-ζ quality basis set is used.

Atomic-projected density of states (DOS) has been calculated (as implemented in Turbomole) by broadening the discrete energy levels of each cluster model with Gaussians having width of 0.003 au and superimposing them.

3. Results and Discussion

3.1. Cluster Models and Local Relaxation Effects. The local relaxation effects in the vicinity of the Pd monomers on PdAu(111) and PdAu(100) clean surfaces have been studied by use of suitably large clusters in order to obtain more realistic models for the chemisorption study of CO molecules.

Locally relaxed structures obtained for the pure gold Au_{57} and Au_{64} cluster models and the bimetallic Pd_2Au_{55} and Pd_2Au_{62} large clusters were compared by use of the BP86 functional, and significant rearrangements have been observed in the active sites as a consequence of the substitution of two noncontiguous surface gold atoms with two Pd monomers. In the surface plane, the neighboring gold atoms move toward the palladium monomers (see Figure 1), whereas on the axis perpendicular to the surface, the Pd atoms move inward (by 0.16−0.20 Å) with respect to the surface gold layer.

As a result of these local relaxations, the Pd−Au distances in the active sites become shorter with respect to the Au−Au distances in the pure gold surfaces. In particular, Pd−Au distances are equal to 2.840 and 2.861 Å for the PdAu(100) and (111) surfaces, respectively. These values differ by 0.017−0.026 Å from the Au−Au distances found with the locally relaxed pure gold clusters. That is an indication of a stronger Pd−Au bond with respect to the Au−Au bond, which is in agreement with the outcome of the study carried out on Pd monomer formation on an Au(111) surface by the slab supercell approach.[33] Moreover, in line with the periodic calculations, weak hybridization between palladium and gold d-orbitals is deducible by the atomic-projected density of states (DOS) plots. In Figure 2, atomic-projected DOS plots of the gold and palladium d-bands, calculated with the BP86 xc functional, for the largest Pd_2Au_{55}(24,21,12) and Pd_2Au_{62}(30,21,13) clusters and the selected Pd_2Au_{19}(12,9) and Pd_2Au_{28}(14,8,8) models are depicted.

When the projected density of d-states for the Pd atom and the nearest gold neighbor atoms is plotted, a wide d-band for gold atoms and a narrow d-band well below the Fermi level for the Pd atom are visible for all cluster calculations.

The main peak of the Pd 4d-band lying at 1 eV below the Fermi level is visible in Figure 2a, whereas in panel b the 5d-band of gold is located between −6.5 and −1.0 eV. These plots, obtained by use of the Pd_2Au_{62}(30,21,13) cluster model, are nicely very close to the results found when a slab supercell was used to represent Pd monomers surrounded by Au atoms in the PdAu(111) surface alloy.[33] It should be noted that in both these DFT calculations a pure xc functional has been used.

When plots obtained for the largest cluster and for the smaller Pd_2Au_{28}(14,8,8) model are compared, both the Pd and Au d-bands appear to be compressed toward the Fermi level in the latter compared to the former. This narrowing of both the metal d-bands, however, does not really affect the overall description of the heterometallic bonds. In fact, for both models (Figure 2a,b) a sharp peak is visible at ∼1.0 eV below the Fermi level, whose low dispersion can be attributed to the strong localization of Pd 4d-electrons, suggesting that the Pd monomer(s) surrounded by gold atoms acquire such atomistic properties. Moreover, the broad 5d-band related to the first-neighbor gold atoms preserves almost the same shape in the two cases even if it shows a different width.

The gold 5d-bands of the Pd_2Au_{28}(14,8,8) and the corresponding Au_{30}(14,8,8) cluster models are depicted in Figure 2b.

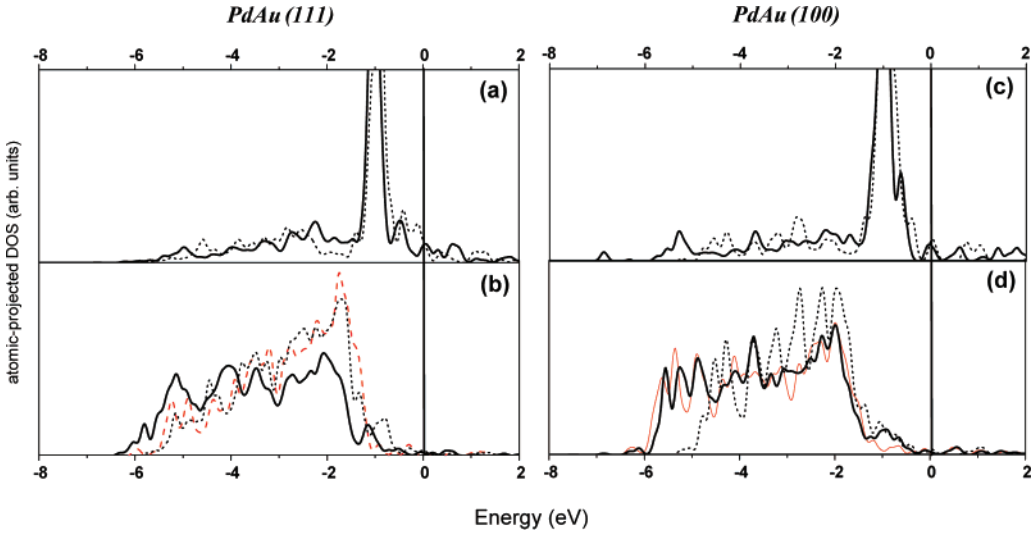

Figure 2. BP86 atomic-projected density of d-states (DOS) of Pd monomers (a, c) and adjacent Au atoms (b, d), calculated for PdAu(111) (a, b) and PdAu(100) (c, d) surface alloys. The largest Pd_2Au_{62}(30,21,13) and Pd_2Au_{55}(24,21,12) cluster models (bold black lines) are compared with selected Pd_2Au_{28}(14,8,8) and Pd_2Au_{19}(12,9) smaller clusters (dotted black lines). Atomic-projected DOS of gold d-states of the clean Au(111) and Au(100) surfaces are calculated for the exemplifying cases of Au_{30} (red dashed line in panel b) and Au_{57} (red thin line in panel d) cluster models. Zero energy is at the Fermi level.

The almost undisturbed Au d-band in the PdAu(111) surface alloy with respect to the pure gold surface (see red dotted line and black dotted line in Figure 2b) and the small overlapping of Pd and Au d-bands in the bimetallic system suggest that a weak orbital hybridization is involved in the Pd−Au bonds.

The projected density of d-states for palladium and gold atoms obtained at the BP86 level in the case of the PdAu(100) surface alloy are reported in Figure 2c,d). No evident differences exist between these plots and what is described above for the PdAu(111) binary system.

The atomic-projected DOS of gold d-band for the PdAu(100) surface alloy (Figure 2d), remains almost unaffected in comparison with the clean Au(100) surface, as in the (111) low-index surfaces.

For simplicity, only the results for the pure gold Au_{57}(24,21,12) and Au_{30}(14,8,8) clusters [modeling the Au(100) and Au(111) gold surfaces, respectively] are reported in Figure 2, but the same indications have been obtained for all remaining Au_{n+2} cluster models.

Comparison between the pictures obtained with the largest Pd_2Au_{55}(24,21,12) and the smallest Pd_2Au_{19}(12,9) cluster models of the PdAu(100) system (Figure 2d) shows a stronger narrowing of the d-bands with respect to the results achieved with the PdAu(111) models (Figure 2b). This comes as no surprise since the description of the electronic properties of the metal surface in the cluster approach is strongly dependent on the cluster size, which is different in these two cases.

3.2. Adsorption of CO Molecules. In order to study the influence of the cluster size on the geometry, vibrational frequencies, and energetics of CO molecules adsorbed on the Pd noncontiguous monomer pairs, a set of six cluster models, as described in the previous section, has been used. In these models the cluster atoms have been kept frozen at their optimized positions, whereas the C and O positions have been fully optimized for all the adsorption sites within the active site. As expected, most of the attempts to find local minima related to the adsorption sites different from those on top of Pd monomers were unsuccessful. This is due to the difference between the chemisorption properties of CO on Pd and Au surfaces, which can be simply explained by the d-band model of Hammer and Nørskov.[54−56] Indeed, the calculated chemisorption energies for CO adsorption atop a metal atom at the Pd(111) and Au(111) metal surfaces are 30.0 and 0.9 kcal/mol, respectively,[57] and then the preferred adsorption site for an ensemble constituted by a Pd monomer surrounded by gold atoms is expected to be the Pd on-top site.

Initially, we started studying the adsorption of one molecule of CO on the six Pd_2Au_n cluster models representing the PdAu(111) and PdAu(100) systems. Energetic, structural, and vibrational properties calculated at the BP86/SVP level of theory for one CO molecule adsorbed on top of one of the two Pd monomers, as a function of the cluster size, are reported in Table 1.

Both experimental data and theoretical results from periodic supercell calculations for adsorption of CO on PdAu(111) surface alloy are available for comparison with our cluster models. In a very recent work, Li et al.,[28] using the Redhead equation (assuming a desorption pre-exponential factor of 1×10^{13} s^{-1}), calculated the desorption activation energy for the Pd atop site on the Au/Pd(111) alloy to be between 18.2 and 20.5 kcal/mol. This result is in good agreement with the binding energies obtained with the Pd_2Au_{28} and the Pd_2Au_{62} cluster models. The corresponding infrared feature found in the RAIRS experiment lies between 2086 and 2089 cm^{-1}, which is comparable to the vibrational frequencies obtained with the Pd_2Au_{28} and Pd_2Au_{62} cluster models (2068 and 2073 cm^{-1}, respectively). In contrast to the work of Li et al.,[28] who deposited a thin film of gold onto a Pd(111) single crystal and heated it to various temperatures, PdAu surface alloys have been generated by other strategies.[5,26] The calculated vibrational and energetic properties obtained with the converged three-layer Pd_2Au_{28} and Pd_2Au_{62} cluster models are also in good agreement with the experimental results of Goodman and co-workers[5,26] reported in these two works.

The only available experimental value of the Pd−CO stretching frequency for PdAu(111) is given by Gleich et al.,[58] who assigned the 371 and 2080 cm^{-1} vibrational peaks of the HREEL spectra to the Pd−C and C−O stretching frequencies, respectively, for CO adsorbed on Pd atoms adjacent to one or more Au surface atoms. As well as for the other calculated properties, these experimental values of the Pd−CO stretching frequency are close to the calculated values obtained by use of

TABLE 1: BP86/SVP Results for Adsorption of One CO Molecule on PdAu Cluster Models[a]

cluster model	BE, kcal/mol	d(Pd−C), Å	ω(Pd−CO), cm^{-1}	d(C−O), Å	ω^{corr}(C−O), cm^{-1}
			hkl (111)		
Pd_2Au_{20}(14,8)	33.6	1.883	454	1.155	2070
Pd_2Au_{28}(14,8,8)	20.0	1.931	383	1.153	2073
Pd_2Au_{62}(30,21,13)	19.3	1.937	378	1.154	2068
exp[b−d]	18.2−20.5[b]		371[d]		2086−2089,[b] 2088,[c,e] 2080[d]
theory[f]	25.6−27.0				2043−2056
			hkl (100)		
Pd_2Au_{19}(12,9)	26.2	1.916	410	1.155	2069
Pd_2Au_{23}(12,9,4)	24.4	1.924	397	1.155	2068
Pd_2Au_{55}(24,21,12)	25.5	1.922	400	1.154	2065
exp[c]					2090−2104

[a] Binding energies (BE) are BSSE-corrected. Scaled C−O frequencies are indicated as ω^{corr}. [b] Reference 28. [c] Reference 5. [d] Reference 57. [e] Reference 59. [f] Reference 33.

the Pd_2Au_{28} and Pd_2Au_{62} cluster models (378 and 383 cm^{-1}, respectively).

The DFT results obtained very recently by Yuan et al.[33] using the slab supercell approach reveal the favorable existence of second-neighbor ensembles. For the adsorption of CO on top of Pd monomers and noncontiguous dimers and trimers, the calculated C−O stretching frequencies show a deviation of 40 cm^{-1} compared to the experimental value, which is twice the deviation obtained with our cluster models. The corresponding adsorption energies for CO adsorbed on the atop sites are 25.6−27.0 kcal/mol at the GGA-PW91 level of theory, which differs by ∼7 kcal/mol from experimental data and our cluster model results. As suggested by the authors, the overestimation of the adsorption energies at the GGA-PW91 level can be corrected by use of the RPBE functional, which is predicted to reduce the values by just 5−7 kcal/ mol.

As already mentioned above, any attempt to reach local minima for bridge or hpc and fcc hollow sites was unsuccessful in accordance with the preferred site found for CO adsorbed on Pd monomers and noncontiguous dimers and trimers by periodic calculations, which is always a Pd atop site.[33]

In view of the converged results reached with the Pd_2Au_{28} and Pd_2Au_{62} cluster models and the agreement with the available experimental data and theoretical results from periodic supercell calculations, one can conclude that the chemical properties of the CO molecule chemisorbed on a Pd monomer in the Pd/Au(111) surface alloy cannot be properly achieved by using the bilayer Pd_2Au_{20}(14,8) cluster model.

On the other hand, for the adsorption of a CO molecule on the more open PdAu(100) surface, we have found a nice convergence of the binding energies using all the cluster models built up for this system (see Table 1).

No local minima have been found for CO adsorbed on bridge Pd−Au sites on the cluster models used to represent the PdAu(100) system, whereas we have found a stable CO chemisorption state on the 4-fold hollow site, in contrast with what has been found for the 3-fold hollow sites in the PdAu(111) surface alloy. This is probably due to the fact that both the Pd monomers of the second-neighbor Pd pair are included in the 4-fold hollow site on the PdAu(100) surface, whereas on the PdAu(111) surface the 3-fold hpc and fcc hollow sites include only one Pd monomer. However, the calculated binding energy for CO adsorbed on the 4-fold hollow site on Pd_2Au_{55}(24,21,12) cluster, at BP86/SVP level, is only 12.2 kcal/mol and the perpendicular distance between the C atom and the surface plane is 1.150 Å, while the d(Pd−C) is 2.428 Å. The C−O distance is 1.182 Å and the corresponding stretching frequency (1788 cm^{-1}) is in the classical region of CO adsorbed on a multifold adsorption site.

As for the CO adsorption on top of a Pd monomer site, all the Pd_2Au_n cluster models built up for the PdAu(100) system give converged results for the CO chemisorption properties on the 4-fold hollow adsorption site. The chemisorption binding energies of CO on the hollow site resulting from all the PdAu(100) cluster models are always less than half the chemisorption energies calculated for the atop adsorption site.

Since no multifold chemisorbed states have been found on the PdAu(111) cluster models and only one less-preferred (4-fold) chemisorbed state has been found on the PdAu(100) cluster models, we will focus for the rest of this paper on the adsorption of CO on top of the Pd monomers.

The results for the adsorption of two CO molecules on top of two noncontiguous Pd monomers by use of our six cluster models are shown in Table 2.

Comparing these results with the chemisorption of one CO molecule, we practically look at two situations with two different CO coverages, and then a rough evaluation of the lateral interaction mediated by the surface can be achieved by calculating the differences between the binding energies per bond in the two cases.

As a first result, it is evident that the same considerations made for the adsorption of one CO molecule regarding the convergence properties of the used cluster models are still valid here and, in general, very small changes have been observed for all the geometrical and vibrational parameters when going from the adsorption of one to two CO molecules.

Since the calculated lateral interactions are, in general, less than 2 kcal/mol per bond (see Table 2) and the effect on the vibrational and geometrical parameters is negligible, all the calculated chemisorption properties of CO on top of Pd monomer are almost unaffected by the presence of other CO molecules on top of a second-neighbor Pd monomer. These results are in line with the experimental observation of very small dipole−dipole coupling between CO molecules on the PdAu surface alloys due to the relatively large intermolecular distance at low coverage regimes (<0.5 ML) and to the improbable adsorption on Au atoms surrounding Pd monomers at higher CO coverages.[59]

3.3. Analysis of the Chemisorption Bond. The Blyholder model[60] is the simplest and most commonly accepted picture for understanding the chemisorption mechanism of CO on metal surfaces. In the spirit of the frontier orbital theory, in that only the highest occupied and lowest unoccupied molecular orbitals (HOMO and LUMO) of the adsorbed molecule are involved in the chemisorption bonding, this model considers only the 5σ donation and the 2π* back-donation contributions to the CO−metal interaction.

TABLE 2: BP86/SVP Results for the Adsorption of Two CO Molecules on PdAu Cluster Models[a]

cluster model	BE, kcal mol^{-1} (CO molecule)$^{-1}$	ΔBE	d(Pd−C), Å	ω(Pd−CO)$_{in}$, cm^{-1}	ω(Pd−CO)$_{out}$, cm^{-1}	d(C−O), Å	ω^{corr} (C−O)$_{in}$, cm^{-1}	ω^{corr} (C−O)$_{out}$, cm^{-1}
					hkl (111)			
Pd_2Au_{20}	24.6	9.0	1.894	460	394	1.155	2079	2065
Pd_2Au_{28}	18.8	1.2	1.938	384	364	1.153	2070	2060
Pd_2Au_{62}	17.0	1.3	1.936	372	360	1.154	2067	2057
exp[b−d]	18.2−20.5[b]			371[d]			2086−2089,[b] 2088,[c,e] 2080[d]	
theory[f]	25.6−27.0						2043−2056	
					hkl (100)			
Pd_2Au_{19}	23.5	2.7	1.924	391	371	1.155	2063	2056
Pd_2Au_{23}	22.6	1.8	1.927	383	373	1.155	2067	2055
Pd_2Au_{55}	23.9	1.6	1.922	406	399	1.154	2068	2056
exp[c]							2090−2104	

[a] BSSE-corrected binding energies per bond are calculated as BE = $[E_{(cluster-(CO)_n)} - nE_{(CO)} - E_{(cluster)}]/n$, where n is the number of CO molecules. With this definition, BE values are in kilocalories per mole per CO molecule. ΔBE is the difference from the BE values in Table 1. (in, out) In-phase and out-of-phase modes of Pd−CO (ω) and scaled C−O (ω^{corr}) stretching frequencies. [b] Reference 28. [c] Reference 5. [d] Reference 57. [e] Reference 59. [f] Reference 33.

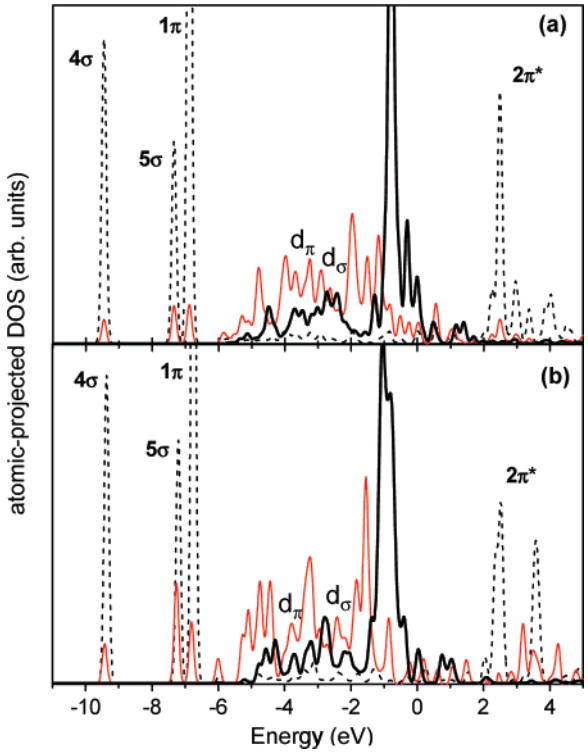

Figure 3. Atomic-projected DOS of Pd d-states (red thin lines) and CO (dotted black lines) in the (a) CO/Pd_2Au_{28}(14,8,8) and (b) CO/Pd_2Au_{19}(12,9) cluster models, together with the atomic-projected density of d-states of Pd (bold black lines) in the corresponding clean PdAu(111) and PdAu(100) surfaces. Zero energy is at the Fermi level.

The atomic-projected DOS for the CO/Pd_2Au_{28}(14,8,8) and the CO/Pd_2Au_{19}(12,9) cluster models, at the BP86/SVP level, are depicted in Figure 3. In both the CO/PdAu(111) and CO/PdAu(100) systems we have found that Pd d-states are strongly disturbed by CO (see Figure 3 a,b). Besides, a relevant shift to lower energies and depletion of the 5σ along with a broadening of the 2π* peak are clearly visible, in accordance with the common donation and back-donation picture. The plots in Figure 3a are in line with the mechanism of CO−PdAu(111) interaction proposed by periodic calculations.[33]

But, as shown by several experimental and theoretical studies,[36,37,61,62] the Blyholder model has some deficiencies and lacks some important subtleties that would be taken into account.

The resonant features at −9.4 and −6.8 eV and in the region between −6.0 eV and the Fermi level in Figure 3 suggest that not only the HOMO and LUMO are involved in the Pd−CO chemical bond and that other minor contributions are given by the 4σ and the 1π CO molecular orbitals along with the formation of new orbital states below the Fermi level (d_σ and d_π bands).

Polarization of the CO−σ system has been observed that can be interpreted as due to a Pauli repulsion between the CO−σ system and the Pd states as already suggested for Ni and Cu clean metal surfaces.[36,37,63] More details on the atomic C and O contributions to the adsorbed CO states are provided as Supporting Information. On the other hand, the interaction between the CO−π system and the 4d Pd states is more complicated and spans three different energy ranges according to the position of bonding, nonbonding, and antibonding states. A detailed description of these contributions to the substrate−adsorbate bond can be found as Supporting Information.

For the Pd monomer ensemble in the PdAu(111) and PdAu(100) surface alloys, the same chemisorption mechanism has been singled out as it is deducible from the comparison of CO/Pd_2Au_{28}(14,8,8) and CO/Pd_2Au_{19}(12,9) systems in Figure 3. The different CO binding energies obtained for these two cluster models (20.0 and 26.2 kcal/mol at the BP86/SVP level, respectively) can be explained by looking at the different contributions of the Pd d-orbitals to the 4σ, 5σ, and 1π bonding orbitals, indicating a more efficient chemisorption process for the PdAu(100) system.

The same information on the chemisorption bond, mainly characterized by orbital overlaps of σ character and relatively small π contributions, has been obtained by analysis on the largest cluster models used for both the PdAu(111) and PdAu(100) surface alloys.

3.4. Exchange−Correlation Functional and Basis-Set Effects. In order to set up suitable quantum-mechanical models for the study of CO adsorption on PdAu bimetallic surfaces, we have studied the influence of the exchange−correlation functional on the electronic properties of PdAu cluster models and the calculated chemisorption properties. For this purpose we have employed the hybrid B3LYP functional. In addition, we have improved the description of the CO electrons by using the TZVP basis set for both BP86 and B3LYP computations.

When local relaxation effects are studied at the B3LYP level, almost the same results with respect to BP86 calculations are obtained. Indeed, Pd−Au distances are equal to 2.832 and 2.854 Å for the PdAu(100) and (111) surfaces, respectively. Moreover, nearly the same description of the Pd−Au bond is obtained, as showed in Figure 4, with the exception of a rigid downshift of both Pd and Au d-bands of 0.7−0.8 eV compared to the BP86 results.

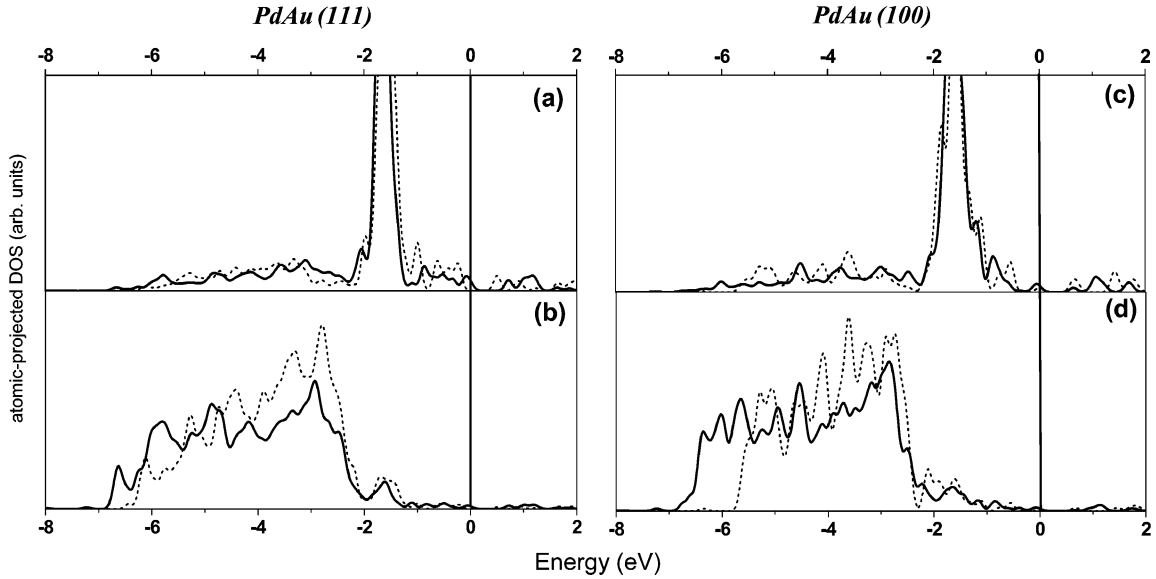

Figure 4. B3LYP atomic-projected density of d-states of Pd monomers (a, c) and adjacent Au atoms (b, d), calculated for PdAu(111) (a, b) and PdAu(100) (c, d) surface alloys. The largest Pd_2Au_{62}(30,21,13) and Pd_2Au_{55}(24,21,12) cluster models (bold black lines) are compared with selected Pd_2Au_{28}(14,8,8) and Pd_2Au_{19}(12,9) smaller clusters (dotted black lines). Zero energy is at the Fermi level.

TABLE 3: BP86/SVP, BP86/TZVP, B3LYP/SVP, and B3LYP/TZVP Results for Adsorption of One CO Molecule on Pd_2Au_{19}(12,9) and Pd_2Au_{28}(14,8,8) Cluster Models[a]

xc functional	basis set	BE, kcal/mol	d(Pd−C), Å	ω(Pd−C), cm^{-1}	d(C−O), Å	ω^{corr}(C−O), cm^{-1}	d(C−O),[b] Å	ω(C−O),[b] cm^{-1}
				Pd_2Au_{19}(12,9)				
BP86	SVP	26.2	1.916	410	1.155	2069	1.142	2152
BP86	TZVP	24.7	1.915	401	1.151	2077	1.138	2128
B3LYP	SVP	17.6	1.944	373	1.141	2069	1.130	2242
B3LYP	TZVP	15.9	1.956	355	1.136	2079	1.127	2216
exp[c,d]						2090−2104[c]	1.128[d]	2170[d]
				Pd_2Au_{28}(14,8,8)				
BP86	SVP	20.0	1.931	385	1.153	2073		
BP86	TZVP	18.5	1.938	370	1.149	2085		
B3LYP	SVP	13.7	1.952	362	1.139	2078		
B3LYP	TZVP	12.0	1.967	344	1.135	2090		
exp[c,e,f]		18.2−20.5[e]		371[f]		2086−2089,[e] 2088,[c] 2080[f]		
theory[g]		25.6−27.0				2043−2056		

[a] Binding energies (BE) are BSSE-corrected. [b] Values for the free CO molecule in the gas phase. [c] Reference 5. [d] Reference 65. [e] Reference 28. [f] Reference 57. [g] Reference 33.

This difference is exclusively due to the different evaluation of the exchange in these two xc functionals and has no effect on the description of the Pd−Au bonds in the surface alloys. Furthermore, by use of both pure and hybrid xc functionals, the electronic configurations and natural charges of the involved atoms in the studied cluster models suggest the same picture for the heterometallic bond; that is, a small amount (0.20−0.25 electron/atom) of Au-to-Pd charge transfer and a small gain of d electrons for Pd atoms in line with other theoretical[33] and experimental[64] works.

Due to the increased computational cost of using a larger basis set and a hybrid exchange−correlation functional, the study of the chemisorption properties has been performed only for the minimal reliable clusters chosen according to the results of the BE convergence studies for both the low-index surface alloys. Therefore, we have chosen the CO/Pd_2Au_{19}(12,9) and CO/Pd_2Au_{28}(14,8,8) cluster models for the PdAu(111) and PdAu(100) surface alloys, respectively. The results for this study are collected in Table 3.

The choice of a triple-ζ quality basis set has an influence of only 1.5 kcal/mol on BP86 binding energies and slightly affects the geometrical parameters. Calculated Pd−CO and C−O stretching frequencies are properly shifted, becoming very close to the experimental available data.

Using the hybrid B3LYP functional, we have found an overall underestimation of the binding energies with respect to the experimental data, whereas a small improvement of the calculated vibrational frequencies, with respect to the BP86 results, has been found.

The differences between the binding energies of CO adsorbed on top of a Pd monomer surrounded by gold atoms, using these two different exchange−correlation functionals, are mainly due to the differently calculated HOMO and LUMO of the CO molecule. In fact, the HOMO and LUMO gaps are smaller in BP86 than in B3LYP, and the HOMO and LUMO are closer to the Fermi energy (see Figure 5 a,b). Hence, following the Blyholder model, the use of the pure xc functional will favor more donation from the 5σ orbital to metal d-states and back-donation from them to the 2π* orbital, since the interaction strength between two states is inversely proportional to their energy separation.

The atomic-projected DOS for the CO*−Pd_2Au_{19}(12,9) noninteracting system (where CO* indicates that the CO molecule is located at 4 Å above the substrate) (Figure 5 a,b) and the CO/Pd_2Au_{19}(12,9) adsorbate/cluster model (Figure 5 c,d) are compared in Figure 5, for both BP86/SVP and B3LYP/SVP levels of theory.

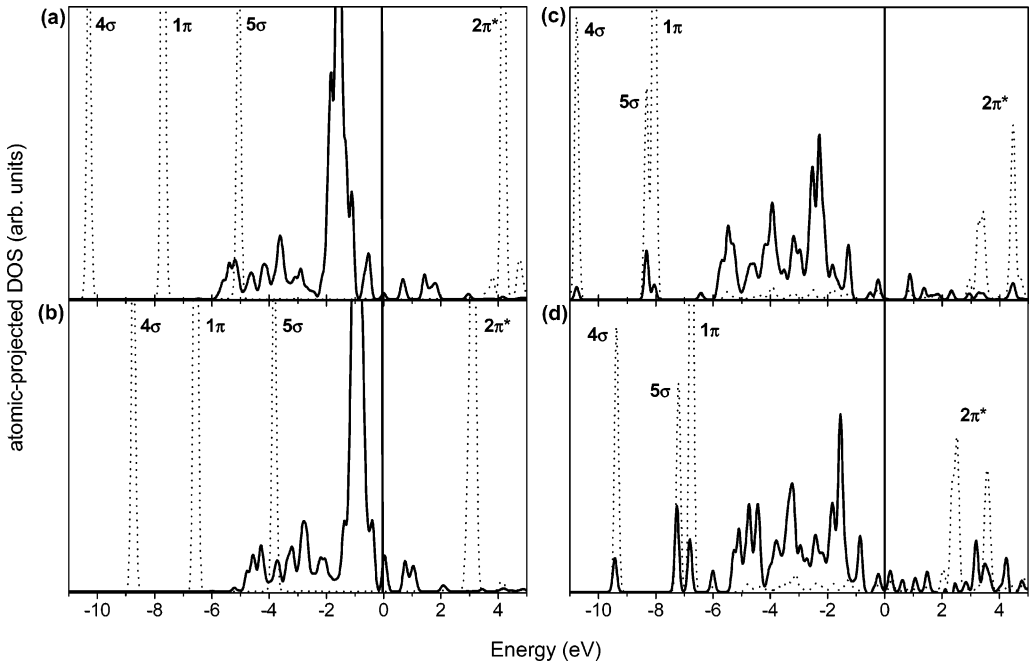

Figure 5. Atomic-projected DOS of Pd (bold lines) and CO (dotted lines) in the CO*/PdAu(100) noninteracting system (a, b) and the CO/PdAu(100) chemisorbed system (c, d). CO* indicates the CO molecule located 4 Å above the Pd monomer in the PdAu(100) surface. Calculations have been performed with Pd_2Au_{19}(12,9) cluster models at the B3LYP/SVP (a, c) and the BP86/SVP (b, d) levels of theory. Zero energy is at the Fermi level.

In the noninteracting CO*−Pd_2Au_{19}(12,9) system, the energy separation between the 4σ, 5σ, and 1π CO molecular orbitals and the main peak of the Pd 4d-band is strongly dependent on the xc functional employed as well as on the position of the antibonding 2π* state above the Fermi level.

Although the overall chemisorption mechanism obtained with the pure xc functional is maintained, the addition of exact exchange seems to lead to a less efficient chemisorption process with a resulting decrease of the Pd−CO binding energies. A possible explanation of this behavior is given as Supporting Information.

The influence of the basis set on the theoretical results at B3LYP level is, in general, similar to what has been found with the BP86 functional. That is, binding energies slightly decrease for both surface alloy models, and C−O and Pd−CO vibrational frequencies come closer to the experimental values (Table 3).

In summary, the use of a more extended basis set is necessary only for an accurate calculation of the vibrational frequencies but is not strictly required for the prediction of chemisorption binding energy trends if the BSSE corrections are included. Moreover, both standard and extended basis sets give the same qualitative description of the chemisorption mechanism, whatever xc functional is used. The admixture of the exact exchange into the xc functional does not have a remarkable influence on the characterization of the heterometallic bond within PdAu surface alloys. The chemisorption binding energies, instead, are strongly dependent on the xc functional used, with the BP86 results better matching the experimental data.

4. Conclusions

In this work we have studied the adsorption properties of CO on the PdAu(111) and PdAu(100) surface alloys by the DF cluster model approach. In particular, cluster models have been built up to represent second-neighbor Pd pair ensembles on both the exposed surfaces.

The local relaxation effects in the active sites have been studied by use of suitably large clusters with sizes of around 60 metal atoms, in order to obtain the more realistic models for the chemisorption study of CO molecules.

Investigation of the chemical properties of the heterometallic bond in the PdAu surface alloys, using these very large clusters, has shown that the Pd−Au bond is stronger than the Au−Au bond and has a slightly ionic character, in line with previous observations.

The energetic and vibrational properties of the CO molecule adsorbed on the PdAu(111) and PdAu(100) surface alloys have been successfully compared with the available theoretical and experimental data. The convergence study of the chemisorption binding energies has showed good reliability of the models with medium cluster size for the calculation of CO chemisorption properties. That has allowed us to study the influence of the exchange−correlation functional and the basis-set quality on the theoretical results with a reasonable computational cost.

The chemisorption mechanism of CO on top of a Pd monomer surrounded by gold atoms has been analyzed by an atom-projected description of the surface chemical bond providing an accurate picture.

The success of the adopted strategy demonstrates that the cluster model approach can be fruitfully employed for the chemisorption study of small molecules on relatively simple critical ensembles of bimetallic surfaces, such as second-neighbor Pd pairs on palladium−gold catalysts.

Acknowledgment. We thank the Università della Calabria for financial support.

Supporting Information Available: Details on the chemisorption mechanism of CO on PdAu(100) surface, influence of the exact exchange on the Pd−CO interaction strength, and metal contribution to the Pd−CO orbitals as a function of the xc functional. This material is available free of charge via the Internet at http://pubs.acs.org.

References and Notes

(1) Sinfelt, J. H. *Bimetallic Catalysts: Discoveries, Concepts and Applications*; Wiley: New York, 1983.

(2) Moss, R. L.; Whally, L. *Advances in Catalysis*; Academic Press: New York, 1972.

(3) Ponec, V. *Adv. Catal.* **1983**, *32*, 149.

(4) Nascimento, M. A. C. *Theoretical aspects of heterogeneous catalysis*; Kluwer Academic Publishers: Dordrecht, The Netherlands, 2001; Vol. 8.

(5) Chen, M.; Kumar, D.; Yi, C. W.; Goodman, D. W. *Science* **2005**, *310*, 291 and supporting online material.

(6) Maroun, F.; Ozanam, F.; Magnussen, O. M.; Behm, R. J. *Science* **2001**, *293*, 1811.

(7) Bligaard, T.; Nørskov, J. K. *Electrochim. Acta* **2007**, *52*, 5512.

(8) Baddeley, C. J.; Tikhov, M.; Hardacre, C.; Lomas, J. R.; Lambert, R. M. *J. Phys. Chem.* **1996**, *100*, 2189.

(9) Baddeley, C. J.; Ormerod, R. M.; Stephenson, A. W.; Lambert, R. M. *J. Phys. Chem.* **1995**, *99*, 5146.

(10) Han, Y. F.; Kumar, D.; Goodman, D. W. *J. Catal.* **2005**, *230*, 353.

(11) Enache, D. I.; Edwards, J. K.; Landon, P.; Solsona-Espriu, B.; Carley, A. F.; et al. *Science* **2006**, *311*, 362.

(12) Trimm, D. L.; Onsan, Z. I. *Catal. Rev.* **2001**, *43*, 31.

(13) Bonarowska, M.; Malinowski, A.; Juszczyk, W.; Karpinski, Z. *Appl. Catal., B* **2001**, *30*, 187.

(14) Rodriguez, J. A. *Surf. Sci. Rep.* **1996**, *24*, (7−8), 225.

(15) Sarkany, A.; Horvath, A.; Beck, A. *Appl. Catal., A* **2002**, *229*, 117.

(16) Hilaire, L.; Legare, P.; Holl, Y.; Maire, G. *Surf. Sci.* **1981**, *103*, 125.

(17) Jablonski, A.; Overbury, S. H.; Somorjai, G. A. *Surf. Sci.* **1977**, *65*, 578.

(18) Swartzfager, D. G.; Ziemecki, S. B.; Kelley, M. J. *J. Vac. Sci. Technol.* **1981**, *19*, 185.

(19) Wood, B. J.; Wise, H. *Surf. Sci.* **1975**, *52*, 151.

(20) Michaelson, H. B. *J. Appl. Phys.* **1977**, *48*, 4729.

(21) Lambert, S.; Heinrichs, B.; Brasseur, A.; Rulmont, A.; Pirard, J. P. *Appl. Catal., A* **2004**, *270*, 201.

(22) Wouda, P. T.; Schmid, M.; Nieuwenhuys, B. E.; Varga, P. *Surf. Sci.* **1998**, *417*, 292.

(23) Kuntze, J.; Speller, S.; Heiland, W.; Deurinck, P.; Creemers, C.; Atrei, A.; Bardi, U. *Phys. Rev. B* **1999**, *60*, 9010.

(24) Kaszkur, Z. *Phys. Chem. Chem. Phys.* **2004**, *6*, 193.

(25) Løvvik, O. M. *Surf. Sci.* **2005**, *583*, 100.

(26) Yi, C. W.; Luo, K.; Wei, T.; Goodman, D. W. *J. Phys. Chem. B* **2005**, *109*, 18535.

(27) Baddeley, C. J.; Barnes, C. J.; Wander, A.; Ormerod, R. M.; King, D. A.; Lamerod, R. M. *Surf. Sci.* **1994**, *1*, 314.

(28) Li, Z.; Gao, F.; Wang, Y.; Calaza, F.; Burkholder, L.; Tysoe, W. T. *Surf. Sci.* **2007**, *601*, 1898.

(29) Gross, A. *Top. Catal.* **2006**, *37*, 1.

(30) Besenbacher, F.; Chorkendorff, I.; Clausen, B. S.; Hammer, B.; Molenbroek, A. M.; Nørskov, J. K.; Stensgaard, I. *Science* **1998**, *279*, 1913.

(31) Kratzer, P.; Hammer, B.; Norskøv, J. K. *J. Chem. Phys.* **1996**, *105*, 5595.

(32) Larsen, J. H.; Chorkendorff, I. *Surf. Sci.* **1999**, *35*, 165.

(33) Yuan, D.; Gong, X.; Wu, R. *Phys. Rev. B* **2007**, *75*, 085428.

(34) Siegbahn, P. E. M.; Wahlgren U.; Schustorovich, E. *Metal−Surface Reaction Energetics*; VCH Publishers: New York, 1991.

(35) Gil, A.; Clotet, A.; Ricart, J. M.; Kresse, G.; Garcìa-Hernàndez, M.; Rosch, N.; Sautet, P. *Surf. Sci.* **2003**, *530*, 71.

(36) Fohlisch, A.; Nyberg, M.; Hasselstrom, J.; Karis, O.; Pettersson, L. G. M.; Nilsson, A. *Phys. Rev. Lett.* **2000**, *85*, 3309.

(37) Fohlisch, A.; Nyberg, M.; Bennich, P.; Triguero, L.; Hasselstrom, J.; Karis, O.; Pettersson, L. G. M.; Nilsson, A. *J. Chem. Phys.* **2000**, *112*, 1946.

(38) Swang, O.; Baerends, E. J.; Fægri, K., Jr.; Gropen, O. *J. Mol. Struct.: THEOCHEM* **1996**, *388*, 321.

(39) Illas, F.; Lòpez, N.; Clotet, A.; Ricart, J. M.; Fernàndez-Garcìa, M.; Conesa, J. C. *J. Phys. Chem. B* **1998**, *102*, 8017.

(40) Sousa, C.; Bertin, V.; Illias, F. *J. Phys. Chem. B* **2001**, *105*, 1817.

(41) Rochefort, A.; Andzelm, J.; Russo, N.; Salahub, D. R. *J. Am. Chem. Soc.* **1990**, *112*, 8239.

(42) Kumar, D.; Chen, M. S.; Goodman, D. W. *Catal. Today* **2007**, 123, 77.

(43) Ahlrichs, M. Bär; Häser, M.; Horn, H.; Kölmel, C. *Chem. Phys. Lett.* **1989**, *162*, 165.

(44) Becke, A. D. *Phys. Rev. A* **1988**, *38*, 3098.

(45) Perdew, J. P. *Phys. Rev. B* **1986**, *33*, 8822.

(46) Eichkorn, K.; Treutler, O.; Öhm, H.; Häser, M.; Ahlrichs, R. *Chem. Phys. Lett.* **1995**, *240*, 283.

(47) Eichkorn, F.; Weigend, O.; Treutler, Ahlrichs, R. *Theor. Chem. Acc.* **1997**, *97*, 119.

(48) Andrae, D.; Hæussermann, U.; Dolg, M.; Stoll, H.; Preuss, H. *Theor. Chim. Acta* **1990**, *77*, 123.

(49) Schäfer, A.; Horn, H.; Ahlrichs, R. *J. Chem. Phys.* **1992**, *97*, 2571.

(50) Becke, A. D. *J. Chem. Phys.* **1993**, *98*, 5648.

(51) Stephens, P. J.; Devlin, F. J.; Chabalowski, C. F.; Frisch, M. J. *J. Phys. Chem.* **1994**, *98*, 11623.

(52) Schäfer, A.; Huber, C.; Ahlrichs, R. *J. Chem. Phys.* **1994**, *100*, 5829.

(53) Boys, S. F.; Bernardi, F. *Mol. Phys.* **1970**, *19*, 553.

(54) Hammer, B.; Nørskov, J. K. *Surf. Sci.* **1995**, *343*, 211.

(55) Pallassana, V.; Neurock, M.; Hansen, L. B.; Hammer, B.; Nørskov, J. K. *Phys. Rev. B* **1999**, *60*, 6146.

(56) Hammer, B. *Topics Catal.* **2006**, *37*, 3.

(57) Hammer, B.; Morikawa, Y.; Nørskov, J. K. *Phys. Rev. Lett.* **1996**, *60*, 2141.

(58) Gleich, B.; Ruff, M.; Behm, R. J. *Surf. Sci.* **1997**, *386*, 48.

(59) Wei, T.; Wang, J.; Goodman, D. W. *J. Phys. Chem. C* **2007**, *111*, 8781.

(60) Blyholder, G. *J. Phys. Chem.* **1964**, *68*, 2772.

(61) Nilsson, A.; Weinelt, M.; Wiell, T.; Bennich, P.; Karis, O.; Wassdahl, N. *Phys. Rev. Lett.* **1997**, *78*, 2847.

(62) Hammer, B.; Nørskov, J. K. *Adv. Catal.* **2000**, *45*, 71.

(63) Bagus, P. S.; Hermann, K. *Phys. Rev. B* **1986**, *33*, 2987.

(64) Nascente, P. A. P.; de Castro, S. G. C.; Landers, R.; Kleiman, G. G. *Phys. Rev. B* **1991**, *43*, 4659.

(65) Huber, K. P.; Herzberg, G. *Molecular Spectra and Molecular Structure, Constants of Diatomic Molecules*; Van Nostrand: Princeton, NJ, 1979; Vol. IV.